Phenomenological theory of magnetoelectric coupling in granular multiferroics

O. G. Udalov,[1,2] N. M. Chtchelkatchev,[1,3,4] and I. S. Beloborodov[1]

[1]*Department of Physics and Astronomy, California State University Northridge, Northridge, California 91330, USA*

[2]*Institute for Physics of Microstructures, Russian Academy of Science, Nizhny Novgorod 603950, Russia*

[3]*L.D. Landau Institute for Theoretical Physics, Russian Academy of Sciences, 117940 Moscow, Russia*

[4]*Department of Theoretical Physics, Moscow Institute of Physics and Technology, 141700 Moscow, Russia*

(Received 7 October 2014; revised manuscript received 12 June 2015; published 6 July 2015)

We study the coupling between the ferroelectric polarization and the magnetization of a granular ferromagnetic film using a phenomenological model of a combined multiferroic system consisting of a granular ferromagnetic film placed above a ferroelectric (FE) layer. The coupling is due to the screening of the Coulomb interaction in the granular film by the FE layer. Below the FE Curie temperature, the magnetization has a hysteresis as a function of the electric field. Below the magnetic ordering temperature, the polarization has a hysteresis as a function of the magnetic field. We study the magnetoelectric coupling for weak and strong spatial dispersion of the FE layer. The effect of mutual influence decreases with increasing spatial dispersion of the FE layer. For weak dispersion, the strongest coupling occurs in the vicinity of the ferroelectric-paraelectric phase transition. For strong dispersion, the situation is the opposite. We study the magnetoelectric coupling as a function of the distance between the FE layer and the granular film. For large distances, the coupling decays exponentially due to the exponential decrease of the electric field produced by the oscillating charges in the granular ferromagnetic film.

DOI: 10.1103/PhysRevB.92.045406 PACS number(s): 75.70.−i, 68.65.−k, 77.55.Nv

I. INTRODUCTION

Currently, the field of multiferroics and materials possessing a magnetoelectric effect is a very active area of research [1–11]. It promises numerous applications, but provides much more fundamental challenges. A vast variety of different multiferroic materials are currently studied by many groups who are looking for strong magnetoelectric (ME) coupling. Among them are single crystals possessing intrinsic ME coupling [12,13], and composite multiferroics consisting of ferroelectric (FE) and ferromagnetic (FM) layers [14–23].

There are several "classical" mechanisms of ME coupling. In a single-crystal multiferroic, the intrinsic ME coupling appears due to spin-orbit interaction, which couples magnetic moments with the orbital motion of electrons [12,13]. Another mechanism involves the electrostriction effect combined with a dependence of the exchange interaction on the interatomic distance, the so-called "exchange striction" [24,25]. A different type of ME effect appears in crystals with magnetic spiral structures. In composite multiferroics consisting of two different materials, magnetic and ferroelectric, the ME coupling appears at the interface of the FE and FM phases [1]. Usually, the coupling is due to a combination of electrostriction and magnetostriction effects. The ME coupling also appears at the metal ferromagnet and insulator interface. In this system, the electric field can induce a charge accumulation at the FM interface modifying the magnetic anisotropy at the surface [20,21]. This effect also involves the spin-orbit interaction. Another type of combined multiferroics includes a layer of a multiferroic with antiferromagnetic ordering and a ferromagnetic layer [7,8]. In these materials, the exchange bias is controlled by the electric field.

A typical example of a two-component multiferroic is the granular multiferroic materials consisting of magnetic particles embedded into a FE matrix [26–31]. Recently, a novel mechanism of ME coupling involving the interplay of the Coulomb blockade effects, intergrain exchange interaction, and ferroelectric dielectric response was proposed for these materials [32,33]. In contrast to the above "classical" ME coupling mechanisms, this mechanism does not involve the spin-orbit interaction. Similar to the "exchange+striction" mechanism the influence of the electric subsystem on the magnetic subsystem occurs through the control of the exchange interaction. However, the control of the exchange interaction has nothing to do with striction and occurs due to the Coulomb blockade, which governs the overlap of electron wave functions.

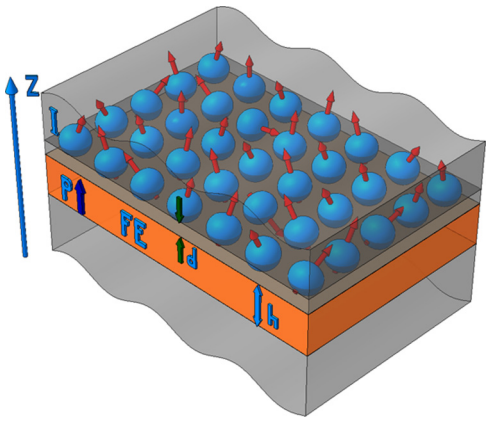

FIG. 1. (Color online) Composite multiferroic material consisting of a granular ferromagnetic film placed at a distance d above the ferroelectric (FE) layer of thickness h. The ferromagnetic film consists of ferromagnetic metallic particles (blue spheres) with finite magnetic moments (red arrows) embedded into an insulating matrix (I). The FE layer has a polarization P along the z axis.

This mechanism was studied using a microscopic theory. In particular, it was shown that the magnetization of granular multiferroics strongly depends on the FE state leading to the appearance of an additional magnetic phase transition in the vicinity of the FE Curie point and to the possibility of controlling the magnetic state of the system by an electric field.

In this paper we study the ME coupling mechanism in a combined granular multiferroic-material consisting of a granular ferromagnetic film (GFM) placed above the FE layer at distance d, see Fig. 1. In contrast to the previous works, here we use a phenomenological approach. This approach allows to account for (i) the spatial dispersion of the FE layer and (ii) the influence of the magnetic subsystem on the FE polarization. Both these effects were not discussed before.

According to Ref. [32], the coupling between the GFM film and the FE layer occurs due to the screening of the Coulomb interaction in the GFM film by the FE layer. The screening was discussed assuming that the FE layer is a dielectric with a local response. In this case, the ME effect has a peak in the vicinity of the FE Curie temperature. However, real FEs have domain walls of finite thickness increasing when approaching the paraelectric-ferroelectric phase transition. The FE layer can not effectively screen the electric field with the characteristic spatial length being smaller than the thickness of the FE domain wall. The characteristic scale for the electric field produced by the GFM film is defined by the intergrain distance. For the FE domain, wall thickness exceeding this scale, so the coupling between the FE and the GFM layers is suppressed. This leads to the decrease of the ME effect in the vicinity of the paraelectric-ferroelectric phase transition, contrary to the local response case. Such a behavior was not discussed before since the ME effect in the GMF film was studied assuming the local response of the FE layer. In this paper, we study the influence of the FE spatial dispersion on coupling between the FE layer and the GFM film.

We use a phenomenological approach to study the system with spatial dispersion. Usually, the ME coupling effects are treated using terms proportional to the product of polarization and magnetization, $\sim\alpha_{\rm me} P^n M^n$ [24]. We describe our system using three phenomenological parameters: (1) the FE polarization, (2) the GFM film magnetization, and (3) the spatial oscillations of charge in the GFM. The later parameter is crucial for granular materials since these materials have complicated morphology leading to the inevitable formation of charge oscillations. We use the local quadrupole moment to describe the system since the average polarization and the average charge in the granular film is zero. The microscopic theory of ME coupling in GMF shows that the charge oscillations are responsible for this coupling, thus supporting the use of these three parameters.

Phenomenologically, the influence of the FE subsystem on the magnetic subsystem is described by the term involving both polarization and magnetization in the total energy of the system [24]. This contribution leads to the inverse effect—the influence of the magnetic subsystem on the FE subsystem. This effect will be discussed in the present paper.

The paper is organized as follows. In Sec. II, we discuss the model for a combined granular multiferroic system. Using this model, we consider the two cases of weak and strong spatial dispersion of the FE layer in Secs. III and IV, respectively. In Sec. V, we discuss the phenomenological and microscopic approaches. Finally, we consider the validity of our approach in Sec. VI.

II. THE MODEL

A. Discussion of ferroelectric substrate state

A uniformly polarized FE layer without domains can be observed between the metallic electrodes with applied bias. These electrodes screen the electric field—this is a well known paradigm verified in numerous experiments.

In our consideration, the FE substrate is placed between the metallic electrode (below the FE substrate) and the granular film (above the FE layer). We assume that the granular film has small but finite conductivity leading to the equilibration of potential in the film. A certain potential U is maintained between the bottom electrode and the granular film. Therefore charges can flow from the bottom electrode to the granular film. The metal electrode and the granular film create an external electric field $E_{\rm ext}$. In addition, bound charges appear at the FE surface. These charges create a depolarizing field $E_{\rm dep}$. The total field acting on the FE due to all these charges is $E_0 = E_{\rm ext} + E_{\rm dep}$. The charges on the bottom electrode and the granular film allow to screen the depolarizing field of the FE substrate surface charges. Thus ferroelectricity with a uniform polarization P_0 locally perpendicular to the film surface exists in the system. We will discuss the domain formation below.

In Ref. [34], it was shown that a granular film effectively screens the depolarizing field of the FE surface charges preventing the suppression of ferroelectricity. As demonstrated in Ref. [34], the Curie temperature of the FE layer decreases slightly in comparison with bulk FE. This may be related to the imperfect screening by the granular film. In Refs. [35,36], it was shown that even one layer of metallic grains effectively screens the electric field.

Here, we note that besides the uniform charge distribution due to the potential applied to the granular film there exist a random distribution of charges among the grains. These charges appear due to impurities and defects inevitably existing in a granular system. Such charges produce a random electric field acting on the FE substrate. This field, however, can hardly be strong enough to induce the formation of FE domains. In equilibrium, the excess charge of the grain related to impurities or defects can hardly be larger than one elementary charge. The field produced by these charges is not strong enough to produce domains in the FE. Often, even ten elementary charges on a typical grain is hardly enough to overcome the typical FE switching field except the very special cases when, for example, the FE is somehow "diluted" [37,38].

Here, we mostly consider the case with all grains having the same charge leading to a uniformly polarized FE. In this case, the average FE polarization is defined by the applied voltage and there are no domains in the FE substrate. However, our results can be also obtained under more general conditions, when in addition to the external field there is a random field of a granular film acting on the FE. In this case, our results remain qualitatively the same until the characteristic length of the random field exceeds the intergrain distance. We will discuss the influence of domains in the next section.

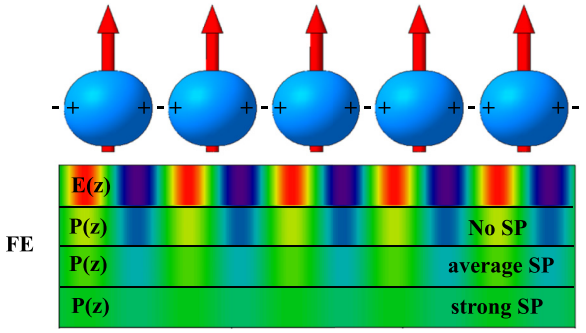

FIG. 2. (Color online) Metallic grains above the FE layer. Due to the complicated morphology, the inhomogeneous spatial charge distribution occurs in the array of grains. This charge distribution produces an electric field in the FE layer [E(z)]. The FE response to this field strongly depends on the spatial dispersion strength in the FE. In the case of weak dispersion, when the domain wall is less than the characteristic field scale, the response is strong (second stripe marked as "No SP"). In the opposite case, the response is suppressed (third stripe marked as "SP").

The electric charges in the granular film also appear in the vicinity of the grain boundaries. These charges appear due to the extension of conduction electron wave functions beyond the grain boundaries. We consider these charges as "regular" charges. On one hand, these charges provide the exchange interaction between grains, and on the another, they interact with the FE substrate via the Coulomb interaction. Namely, these charges are responsible for the ME coupling in our consideration, see Figs. 2 and 3(b). Since the field of these "regular" charges plays the key role in the coupling between the FE layer and the granular film, we use letters E (field intensity) and D (field induction) to describe it. The total field in the FE layer $E_{\rm tot}$ and $D_{\rm tot}$ can be written as follows: $E_{\rm tot} = E_0 + E$ and $D_{\rm tot} = D_0 + D$. The field of "regular" charges is not strong enough to produce domains in the FE, but it leads to a weak variation of the polarization in the substrate, which can be considered as a linear perturbation on the uniform (polarization) background. This polarization correction is defined as $P^{(1)}$, therefore the local polarization at each point can be written as $P = P_0 + P^{(1)}$.

B. Importance of spatial dispersion

In contrast to previous considerations of the ME coupling in a composite FE we take into account the spatial dispersion, when $\mathbf{P}(\mathbf{r}) = \int \chi(\mathbf{r},\mathbf{r}')\mathbf{E}(\mathbf{r}')d\mathbf{r}'$. It plays a crucial role for the ME coupling in the system. The interaction between the granular film and the FE layer is due to the Coulomb interaction. An inhomogeneous spatial distribution of "regular" charges in the granular film produces an inhomogeneous electric field inside the FE layer. This field has a zero average.

Figure 2 shows metallic grains producing an electric field $\mathbf{E}(z)$ inside the FE layer. This field is not strong enough to create domains in the FE (the field amplitude is essentially less than the FE switching field) and can be considered as perturbation. The characteristic length scale of this field is the intergrain distance L. When the spatial dispersion is weak and the characteristic scale of the spatial dispersion $l_{\rm SD}$ (which

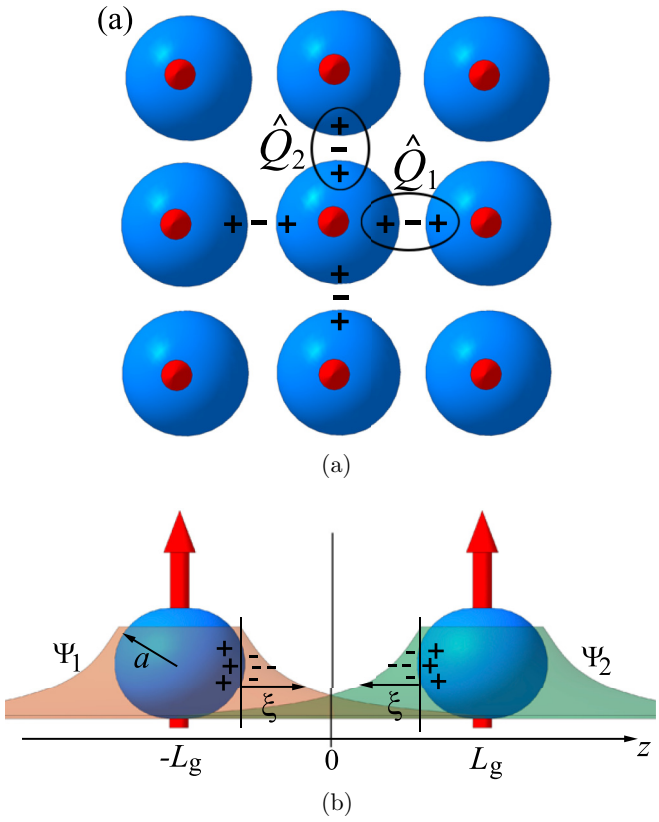

FIG. 3. (Color online) (a) Lattice of metallic grains. The interparticle spacing has a small negative charge and grains have small positive charges due to electron tunneling between grains leading to the formation of quadrupole moments in the regions between grains. There are two types of quadrupoles, $\hat{Q}_1$ and $\hat{Q}_2$. (b) Two magnetic grains. Electron wave functions (Ψ_1 and Ψ_2) extend beyond the grains and overlap in the region between the grains. ξ is the decay length of the electron wave functions. Quadrupole moment appears due to presence of electrons outside the grains. Exchange interaction between grains appears due to the overlap of electron wave functions.

is related to the FE domain wall thickness as $l_{\rm DW} \sim l_{\rm SD}\sqrt{\chi}$) is less than the intergrain distance, the polarization locally follows the electric field. Thus the susceptibility of the FE substrate is $\chi(k) \approx \chi(k=0) = \chi_0$ and for the polarization one has

$$\mathbf{P}_\mathbf{k} \sim \chi_0 \mathbf{E}_\mathbf{k}, \tag{1}$$

see the second stripe ("No SP"). Here, $P_\mathbf{k}$ and $E_\mathbf{k}$ are the spatial Fourier harmonics of the polarization and the electric field, respectively. Thus, in the absence of random electric fields due to random impurities and defects, the susceptibility depends only on the average polarization defined by the bias voltage. In this case, χ is the same over the FE substrate. To summarize: in the absence of spatial dispersion, the FE response is large and the interaction between the GFM and the substrate is strong.

A strong spatial dispersion, $l_{\rm SD} \gg L$ ($|\mathbf{k}|l_{\rm SD} \gg 1$), leads to the suppression of the FE response on the small scale variation of the electric field produced by grains. In this case, one can not neglect the k-dependence of the susceptibility, $\chi(k)$. For large k, $k \to \infty$, the susceptibility $\chi(k) \to 0$. The leading

contribution is quadratic in k due to symmetry reasons:

$$\mathbf{P}_\mathbf{k} \sim \chi(k)\mathbf{E}_\mathbf{k}, \quad \chi(k) \sim \frac{\chi_0}{\mathbf{k}^2 l_{\mathrm{DW}}^2} \tag{2}$$

(third stripe in Fig. 2, "average SD"). This contribution leads to the suppression of interaction between the grains and the FE layer and thus to the suppression of the ME coupling. Finally, the response disappears for very strong dispersion (forth stripe in Fig. 2, "strong SD").

The degree of spatial dispersion in the FE can be different. It depends on the ferroelectric material, temperature, and other parameters. Below, we investigate how the spatial dispersion influences the magnetoelectric coupling in the general case considering the limits of weak and strong spatial dispersions, and we justify the validity of Eq. (2).

We mention that the above estimates are valid for a random electric field, produced by the random charges and defects, being zero. For finite random field, the dielectric susceptibility $\chi(\mathbf{r},\mathbf{r}')$ of the FE film depends slowly on the coordinate $\mathbf{R} = (\mathbf{r}+\mathbf{r}')/2$. Thus, in Fourier space, we have $\chi = \chi(\mathbf{k},\mathbf{R})$. This dependence appears since the local susceptibility depends on the local electric field acting on the FE. In this case, we use an effective dielectric susceptibility averaged over the random field distribution. This effect changes the ME coupling dependence on the bias voltage, however, it does not suppress it until the characteristic spatial scale of the random electric field exceeds the intergrain distance.

C. System parameters

In this section, we discuss the model of composite multiferroics—materials consisting of two thin layers: (i) ferroelectric (FE) layer and (ii) granular ferromagnetic film (GFM) made of ferromagnetic grains embedded into an insulating matrix, see Fig. 1. The grains have average radius a of few nanometers with the distance between grains being 1–2 nm. The distance between the neighboring grain centers is L_g. Each grain is characterized by a large Curie temperature, much larger than all other characteristic energy scales in the problem. Therefore each particle is in the FM state. Due to the interaction between particles, the macroscopic FM state may occur in the GFM film for temperatures $T < T_\mathrm{C}^\mathrm{FM}$, where T_C^FM is the ferromagnetic ordering temperature.

There are three phenomenological parameters characterizing the system: (1) the coordinate dependent electric polarization of the FE layer, $\mathbf{P}$; (2) the average magnetization of the GFM layer, $\mathbf{M}$; (3) the spatial oscillations of electric charge in the GFM film appearing due to the inhomogeneous distribution of metallic inclusions in the granular film, see Fig. 3.

A spatial charge distribution in the granular film has two components: (1) a uniform component. We assume that a voltage difference is maintained between a metal electrode at the bottom of the FE substrate and the granular film. The film has low but finite conductance, leading to the equilibration of potential in the film. A surface charge of the FE substrate is screened by the charges uniformly distributed among grains.

(2) The second component of the spatial charge distribution is the inhomogeneous component. Below, we will concentrate on this component since it is responsible for the coupling between the magnetic moment of the granular film and the FE layer. The electron wave functions extend beyond the metallic grains leading to the appearance of a nonzero local electric dipole moment. Opposite dipole moments of two neighboring grains form a quadrupole moment between each pair of grains. Therefore the system is described by the ensemble of quadrupoles with moments $\hat{Q}_i$, see Fig. 3.

We mention that the importance of electron wave function extension beyond the metallic grains was understood in optics early. This is the so-called "spill-out" effect. For example, due to this effect, the plasmon frequency of the nanograin becomes sensitive to the spilled fraction of electrons: $\omega_\mathrm{pl} = \omega_\mathrm{pl}^{(0)}(1 - \delta N_e/2N_e)$, where δN_e is the spilled electron fraction, N_e is the number of electrons in the nanograin, and $\omega_\mathrm{pl}^{(0)}$ is the bulk material plasma frequency, see, e.g., Ref. [39].

Our system is characterized by several length scales. The domain wall thickness L_p in the FE away from the transition point can be comparable with the interatomic distance. In this case, L_p is smaller than the intergrain distance L_g. Close to the transition point, the situation is the opposite, $L_\mathrm{p} > L_\mathrm{g}$. The magnetic domain wall thickness L_m in the GFM film is much larger than the intergrain distance, $L_\mathrm{m} > L_\mathrm{g}$.

D. Free energy

The total free energy of the system consists of three contributions: (1) the energy of the FE layer, W^FE, (2) the energy of the GFM film, W^GFM, and (3) the interaction energy between two subsystems, W^I. Below we discuss each energy contribution in details.

1. *Energy of granular ferromagnetic film, W^GFM*

The free energy of GFM film, W^GFM has two contributions:

$$W^\mathrm{GFM} = W_\mathrm{m}^\mathrm{GFM} + W_\mathrm{c}^\mathrm{GFM}, \tag{3}$$

where $W_\mathrm{m}^\mathrm{GFM}$ is the energy of the magnetic subsystem [40]:

$$W_\mathrm{m}^\mathrm{GFM} = \alpha_\mathrm{M} M^2 + \beta_\mathrm{M} M^4 - (\mathbf{M}\cdot\mathbf{B}) + \delta_\mathbf{M}(\nabla\mathbf{M})^2. \tag{4}$$

Here, α_M, β_M, δ_M are some phenomenological constants and $\mathbf{B}$ is the external magnetic field.

The second contribution, $W_\mathrm{c}^\mathrm{GFM}$ in Eq. (3) is due to spatial charge oscillations. The simplest model of regular rectangular array of identical grains with the lattice parameter L_g is characterized by the regular array of quadrupoles $\hat{Q}^i$, which can be characterized by the magnitude $Q^i = Q^i_{xx} + Q^i_{yy}$. Below, we consider a uniform spatial distribution of quadrupole moments and introduce a single parameter describing the system of quadrupoles, Q ($Q^i = Q$). There are two types of quadrupoles, $\hat{Q}^1$ and $\hat{Q}^2$, see Fig. 3. These quadrupoles are transformable one into another using the rotation $\pi/2$ ($Q^1_{xx} = Q^2_{yy}$, $Q^1_{yy} = Q^2_{xx}$). Both quadrupoles have the same magnitude Q, however, the electric field produced by these quadrupoles is different.

We define the electrical induction of an electric field produced by a quadrupole with a unit moment ($Q = 1$) as $\mathbf{D}_i^\mathrm{q}(\mathbf{r},\mathbf{r}_i)$, where index i stands for quadrupole i, $\mathbf{r}_i$ denotes the quadrupole position, and $\mathbf{r}$ defines the observer position. Below, we will omit vectors $\mathbf{r}_i$ for simplicity keeping the index i only. There are two different spatial distributions of electric

field $\mathbf{D}_i^{\mathrm{q}}$ corresponding to two types of quadrupoles. The total electric field produced by quadrupoles is $\mathbf{D} = Q\sum_i \mathbf{D}_i^{\mathrm{q}}$.

The phenomenological parameter $\hat{Q}_i$ is different from the polarization $\mathbf{P}$ and the magnetization $\mathbf{M}$ since quadrupoles appear due to the complex morphology and not due to a phase transition. In the absence of magnetization and ferroelectricity, the quadrupoles are described by the following free energy $W_{\mathrm{c}}^0 = \alpha_Q(Q - Q_0)^2$, where Q_0 is the equilibrium magnitude of quadrupoles at a given temperature T and the parameter α_Q depends on temperature.

Quadrupoles interact with each other via the electric field. The energy density of this field is

$$W^{\mathrm{E}} = \frac{Q^2}{8\pi\,\Omega_{\mathrm{GFM}}}\sum_{i,j}\int d^3r\mathbf{D}_i^{\mathrm{q}}(\mathbf{r})\mathbf{D}_j^{\mathrm{q}}(\mathbf{r}), \tag{5}$$

where Ω_{GFM} is the volume of the GFM film. Without loss of generality we assume that beside the FE layer, the dielectric permittivity of all other space is approximately 1. The average electric field produced by the ensemble of quadrupoles is zero. Therefore the interference of the field $\mathbf{E}_0$ and the quadrupole field is negligible, $\int d^3r\mathbf{E}_0\cdot\sum_i D_i^{\mathrm{q}} = 0$.

The spatial charge oscillations produce an additional contribution to the system Coulomb energy W^{GFM}. This contribution defines the coupling between the quadrupoles and the magnetic subsystem. The exchange interaction is a short-range interaction. Thus we use the local coupling between the parameter Q and the magnetization M. Since Q is invariant with respect to the spatial inversion, it enters linearly into the coupling term. Finally, we obtain the following result for the energy of quadrupoles:

$$W_{\mathrm{c}}^{\mathrm{GFM}} = W_{\mathrm{c}}^0 + W^{\mathrm{E}} + \gamma(Q - Q_0)M^2, \tag{6}$$

where γ is a phenomenological parameter. The higher order terms, σ^4M^2, σ^2M^4, and σ^4M^4 can be taken into account as well. For simplicity, we consider only the lowest order coupling term between Q and M. The microscopic origin of this coupling is discussed in Sec. V.

2. Energy of ferroelectric layer, W^{FE}

We consider the case of isotropic FE. The typical example of isotropic FEs are organic ferroelectrics. Our theory can be easily generalized for anisotropic FE. We discuss this point in Sec. VI. The free energy of the FE layer has the form [41–44]

$$W^{\mathrm{FE}} = \alpha_{\mathrm{P}}P^2 + \beta_{\mathrm{P}}P^4 + \delta_{\mathbf{P}}(\nabla\mathbf{P})^2 - (\mathbf{P}\cdot\mathbf{E}_0). \tag{7}$$

Here, α_{P}, $\delta_{\mathbf{P}}$, and β_{P} are phenomenological constants and $\mathbf{E}_0$ is the homogeneous electric field produced by the bound FE charges, granular film, and the bottom electrode. It is directed perpendicular to the FE layer (z axis).

We notice that the charges inside the granular film responsible for the field $\mathbf{E}_0$ and quadrupoles in the GFM film have a different origin: the charges outside the GFM film are created by the voltage source leading to the fixed electric field $\mathbf{E}_0$ but not to the fixed electric induction $\mathbf{D}_0$, while the quadrupoles appear due to the complex morphology producing a finite electric field induction $\mathbf{D}$ rather than the electric field $\mathbf{E}$.

3. Interaction energy between two subsystems, W^{I}

The coupling between the FE layer and the GFM film occurs due to the interaction of the electric field produced by quadrupoles in the GFM film with the FE layer:

$$W^{\mathrm{I}} = -\frac{Q}{2\Omega_{\mathrm{GFM}}}\sum_i\int d^3r\mathbf{D}_i^{\mathrm{q}}(\mathbf{r})\mathbf{P}(\mathbf{r}), \tag{8}$$

where the FE polarization has the form

$$\mathbf{P} = \mathbf{P}_0 + \mathbf{P}^{(1)}(\mathbf{r}) + \mathbf{P}^{(2)}(\mathbf{r}). \tag{9}$$

Here, $\mathbf{P}_0$ is the spontaneous (or external field induced) uniform polarization of the FE layer. It depends on the external field below and above the transition temperature $T_{\mathrm{C}}^{\mathrm{FE}}$. We assume that the electric field created by quadrupoles in the FE layer is weak. The terms $\mathbf{P}^{(1,2)}(\mathbf{r})$ in Eq. (9) are the linear and quadratic responses of the FE to the quadrupoles field $\mathbf{D}$:

$$\mathbf{P}^{(1)}(\mathbf{r}) = Q\sum_i\int_{\Omega_{\mathrm{FE}}} d^3r'\hat{\chi}(\mathbf{r},\mathbf{r}')\mathbf{D}_i^{\mathrm{q}}(\mathbf{r}'), \tag{10}$$

where $\hat{\chi}(\mathbf{r},\mathbf{r}')$ is the linear response function of the FE layer to the electric induction. In general, $\hat{\chi}(\mathbf{r},\mathbf{r}')$ is a tensor depending on the polarization $\mathbf{P}_0$, temperature, and electric field $\mathbf{E}_0$. Inside the FE layer, $\hat{\chi}(\mathbf{r},\mathbf{r}')$ depends on both coordinates $\mathbf{r}$ and $\mathbf{r}'$ due to boundary conditions. In the bulk, the susceptibility depends only on the coordinate difference $(\mathbf{r} - \mathbf{r}')$.

The quadratic response in Eq. (9) has the form

$$\mathbf{P}^{(2)}(\mathbf{r}) = Q^2\sum_{i,j}\int_{\Omega_{\mathrm{FE}}} d^3r'd^3r''\hat{\chi}^{(2)}(\mathbf{r},\mathbf{r}',\mathbf{r}'')\mathbf{D}_i^{\mathrm{q}}(\mathbf{r}')\mathbf{D}_j^{\mathrm{q}}(\mathbf{r}''), \tag{11}$$

where $\hat{\chi}^{(2)}(\mathbf{r},\mathbf{r}',\mathbf{r}'')$ is the contribution to the susceptibility quadratic in the electric induction. Introducing Eq. (10) into Eq. (8), we find for the interaction energy

$$W^{\mathrm{I}} = -\frac{Q^2}{2\Omega_{\mathrm{GFM}}}\sum_{i,j}\int d^3rd^3r'\mathbf{D}_i^{\mathrm{q}}(\mathbf{r})\hat{\chi}(\mathbf{r},\mathbf{r}')\mathbf{D}_j^{\mathrm{q}}(\mathbf{r}'). \tag{12}$$

The quadratic polarization $\mathbf{P}^{(2)}(\mathbf{r})$ does not contribute to the interaction energy W^{I} since it produces an odd-degree oscillating electric field $\mathbf{D}$.

4. Total energy of electric field

The total energy of electric field is given by the following expression:

$$W^{\mathrm{E}} + W^{\mathrm{I}} = Q^2R, \tag{13}$$

where we introduce the notation

$$R = \sum_{i,j}\int d^3rd^3r'\mathbf{D}_i^{\mathrm{q}}(\mathbf{r})\left(\frac{\delta(\mathbf{r} - \mathbf{r}')}{8\pi\,\Omega_{\mathrm{GFM}}} - \frac{\hat{\chi}(\mathbf{r},\mathbf{r}')}{2\Omega_{\mathrm{GFM}}}\right)\mathbf{D}_j^{\mathrm{q}}(\mathbf{r}'). \tag{14}$$

The coefficient R depends on temperature T and the electric field $\mathbf{E}_0$ through the susceptibility $\hat{\chi}(\mathbf{r},\mathbf{r}')$. In addition, the coefficient R also depends on the distance between the GFM film and the FE layer and on the FE thickness.

E. Variational procedure

Minimizing the total energy of the system in parameter Q, we obtain the equation describing the magnitude of the

quadrupole:

$$2\alpha_Q(Q - Q_0) + 2RQ + \gamma M^2 = 0. \quad (15)$$

This equation has the solution

$$Q = \frac{\alpha_Q Q_0 - \gamma M^2/2}{\alpha_Q + R}. \quad (16)$$

We notice that Q depends on both subsystems—the GFM film magnetization and the FE layer polarization through the coefficient R leading to the coupling between the FE polarization P and the GFM magnetization M.

The equation describing the magnetization behavior (up to linear in parameter γ terms) has the form

$$2\tilde{\alpha}_M \mathbf{M} + 4\beta_M M^2 \mathbf{M} = \mathbf{B},$$
$$\tilde{\alpha}_M = \alpha_M - \gamma \frac{RQ_0}{\alpha_Q + R}. \quad (17)$$

The magnetization $\mathbf{M}$ is parallel to the plane of the GFM film. The magnetic field existing at the film edges is negligible due to the large area of the film. We assume that the magnetization $\mathbf{M}$ in Eq. (17) is uniform because the domain wall thickness in the GFM film is much larger than the intergrain distance and the film thickness.

The coefficient $\tilde{\alpha}_M$ depends on the FE state through the coefficient R and has some peculiarities in the vicinity of the FE Curie point due to singularities in the susceptibility $\hat{\chi}(\mathbf{r},\mathbf{r}')$. Since the coefficient R depends on the field $\mathbf{E}_0$, one can control the magnetic state of the GFM film by the electric field. The influence of the GFM film on the FE layer is finite due to the electric field created by quadrupoles.

III. FE WITHOUT SPATIAL DISPERSION

In the absence of spatial dispersion, the FE susceptibility has the form

$$\hat{\chi}(\mathbf{r},\mathbf{r}') = \hat{\chi}\delta(\mathbf{r} - \mathbf{r}'). \quad (18)$$

Substituting this result into Eq. (14), we find the following result for the coefficient R:

$$R = R_0 - \chi_{||} R_{||} - \chi_\perp R_\perp,$$
$$R_0 = \frac{1}{8\pi\Omega_{GFM}} \sum_{i,j} \int d^3r \mathbf{D}^q_i(\mathbf{r}) \mathbf{D}^q_j(\mathbf{r}),$$
$$R_{||} = \frac{1}{2\Omega_{GFM}} \sum_{i,j} \int_{\Omega_{FE}} d^3r D^q_{i(||)}(\mathbf{r}) D^q_{j(||)}(\mathbf{r}),$$
$$R_\perp = \frac{1}{2\Omega_{GFM}} \sum_{i,j} \int_{\Omega_{FE}} d^3r \mathbf{D}^q_{i(\perp)}(\mathbf{r}) \mathbf{D}^q_{j(\perp)}(\mathbf{r}). \quad (19)$$

We assume that the FE layer has the anisotropy axis perpendicular to the layer surface. The quantities $\chi_{||}$ and $\chi_\perp$ describe the longitudinal and perpendicular susceptibility, respectively. The subscripts $||$ and $\perp$ define the longitudinal and perpendicular components of the electric induction.

To find the susceptibility in the absence of spatial dispersion, we need to solve the following equation:

$$2\alpha_P \mathbf{P} + 4\beta_P P^2 \mathbf{P} = \mathbf{E}_0 + \mathbf{E}, \quad (20)$$

which has the solution

$$\mathbf{P}^{(1)} = \hat{\chi}\mathbf{D}, \quad (21)$$

where

$$\chi_{||} = \left(2(\alpha_P + 2\pi) + 12\beta_P P_0^2\right)^{-1},$$
$$\chi_\perp = \left(2(\alpha_P + 2\pi) + 4\beta_P P_0^2\right)^{-1}. \quad (22)$$

It follows from Eq. (22) that for zero field $\mathbf{E}_0$ the susceptibility $\hat{\chi} < 1/(4\pi)$.

A. Influence of FE layer on the GFM film

In this section, we investigate the influence of the FE layer on the magnetic subsystem. In the absence of spatial dispersion of the FE, Eq. (17) has the form

$$2(\alpha^*_M + \gamma_\perp\chi_\perp + \gamma_{||}\chi_{||})\mathbf{M} + 4\beta_M M^2 \mathbf{M} = \mathbf{B}, \quad (23)$$

with the following coefficients:

$$\alpha^*_M = \alpha_M - \gamma R_0 Q_0/\alpha_Q,$$
$$\gamma_\perp = \gamma R_\perp Q_0/\alpha_Q, \quad (24)$$
$$\gamma_{||} = \gamma R_{||} Q_0/\alpha_Q.$$

Equation (24) is valid for $R \ll \alpha_Q$ meaning that the interaction of the GFM with the FE layer leads to the renormalization of the constant α_M. Changing the FE susceptibility $\hat{\chi}(\mathbf{r},\mathbf{r}')$ by the electric field one can change the FM ordering temperature. Since the susceptibility of FE has some peculiarity in the vicinity of the FE Curie point, the magnetic properties of the GFM film should also exhibit some peculiarities in the vicinity of the FE Curie point.

We assume that the coefficient $\alpha^*_M = \tilde{\alpha}^{FM}(T - T_C^{FM})$ in Eq. (24) defines the position of superparamagnetic-ferromagnetic (SPM-FM) phase transition in the GFM film in the absence of a FE layer.

The temperature dependence of the magnetization and the magnetic susceptibility of the GFM film at zero external magnetic field is shown in Fig. 4. Both limits of $T_C^{FE} > T_C^{FM}$ and $T_C^{FM} > T_C^{FE}$ are relevant since the ordering temperature of GFM can be rather large reaching the room temperature [45,46], and because FE's with a Curie point below and above the room temperature exist [47–51].

Figure 4(a) shows the case $T_C^{FM} < T_C^{FE}$, for substrate we choose a colemanite film [50,51]. In contrast to $BaTiO_2$ ferroelectric, the colemanite has a rather small dielectric permittivity, which is important for a granular system since it prevents the total suppression of the Coulomb gap in the granular film. The behavior of colemanite thin films is well described using Landau-Ginzburg-Devonshire theory. The FE Curie temperature is about $T_C^{FE} = 267$ K. We use the experimental data of Ref. [51] on the temperature dependence of the dielectric permittivity to estimate the parameters $\tilde{\alpha}_P = 0.031$ K^{-1} $[\alpha_P = \tilde{\alpha}_P(T - T_C^{FE})]$. To calculate $\tilde{\alpha}_P$, we estimate the slope of the FE inverse susceptibility.

For a magnetic film, we use Ni granular film [45]. At certain concentration of Ni (about 45%), the ordering temperature of this film is about $T_C^{FM} = 100$ K. Using the data of Ref. [45], we can estimate the parameter $\alpha^*_M = 0.02 \cdot (T - T_C^{FM})$ erg/(Oe^{-2}cm^3). The parameter

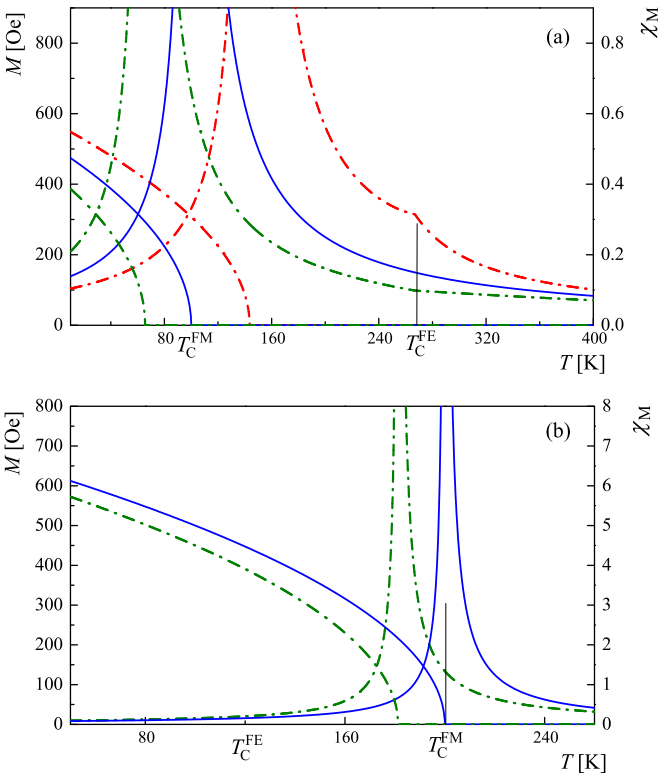

FIG. 4. (Color online) Magnetization M and magnetic susceptibility χ_M vs temperature at zero magnetic and electric fields. Solid (blue) line corresponds to the absence of the FE layer. Dashed (red) line corresponds to negative parameter γ. Dash dotted (green) line corresponds to positive γ. T_C^{FE} and T_C^{FM} are the ordering temperatures of the FE layer and the GFM film in the absence of mutual interaction, respectively. (a) Limit of $T_C^{FE} < T_C^{FM}$. This limit corresponds to colemanite FE substrate and 45% of Ni granular film. (b) Limit of $T_C^{FE} > T_C^{FM}$. This limit corresponds to TTF-CA ferroelectric substrate and 48% of Ni granular film. The interaction of FE and GFM layers leads to the appearance of peculiarities of magnetization M [see panel (a)] and susceptibility χ_M in the vicinity of the FE phase transition.

$\beta_M = 4\times10^{-6}$ erg/(Oe^{-4} cm^3) is not given in Ref. [45]. We take this parameter assuming that the magnetization of the granular film is several times smaller than the magnetization of the bulk Ni; the parameter β_M does not influence the behavior of the magnetization and susceptibility qualitatively.

Similarly, a Co-SiO_2 film can be used. It has similar magnetic parameters but at different metallic concentration [46]. In the case of 23% Co-SiO_2 film, $\alpha_M^* = 0.03\,(T - T_C^{FM})$ with $T_C^{FM} = 93$ K. The parameter can be estimated using the data on the magnetic susceptibility of the Co-SiO_2 film.

To estimate the parameter γ, we use an approach discussed in Sec. V. Figure 4(a) shows the case $\gamma_{||} = -24$ and $\gamma_\perp = -1.6$. We note that the large values of γ lead to a small perturbation of the magnetic properties since the function $\chi_{||,\perp}$ depends on the small parameter $1/(16\pi^2\chi_0^{FE})$, where χ_0^{FE} is the dielectric permittivity of the FE with respect to the electric field. It is related to the susceptibility χ with respect to the electric induction in the following way: $\chi = 1/(4\pi)[1 - 1/(4\pi\chi_0^{FE})]$. An estimate of parameter γ for particular FE and GFM gives a negative coupling constant. We also show the case of positive $\gamma_{||,\perp}$ in Fig. 4(a) (dashed line). According to Sec. V, the constant γ may have values larger than it was used here. In this section, we decrease the parameter γ increasing the distance between the FE and the GFM film.

Figure 4(b) shows the case $T_C^{FM} > T_C^{FE}$. This limit can be realized with a TTF-CA ferroelectric, with a phase transition temperature $T_C^{FE} = 81$ K [52]. This FE has a broader peak of dielectric permittivity in the vicinity of the FE phase transition leading to a low parameter $\tilde{\alpha}_P = 0.001$. The parameter is estimated using the slope of the inverse susceptibility curve provided in Ref. [52]. A large Curie constant leads to the disappearance of peculiarity in the magnetization versus temperature in the vicinity of T_C^{FE}, however, it still leads to an essential shift of the magnetic ordering temperature. In this case, we use a Ni granular film with Ni concentration of 49%, leading to $T_C^{FM} = 200$ K. The parameters $\gamma_{||,\perp}$ are equal to -4 and -0.8, respectively.

The interaction of FE and GFM layers leads to two effects: (1) the shift of the GFM film ordering temperature, which can be estimated as follows:

$$\Delta T = -\frac{\gamma_{||}\chi_{||} + \gamma_\perp\chi_\perp}{\tilde{\alpha}^{FM}}, \tag{25}$$

where $\chi_{||,\perp}$ is taken in the vicinity of the transition temperature T_C^{FM}. The shift direction depends on the sign of interaction.

(2) The peculiarity of magnetization and magnetic susceptibility in the vicinity of the FE phase transition. The maximum deviation of magnetic susceptibility occurs at the FE phase transition point. For $T_C^{FE} > T_C^{FM}$, it has the form

$$\Delta\chi_M = -\frac{\gamma_{||}\chi_{||} + \gamma_\perp\chi_\perp}{2\left[\tilde{\alpha}^{FM}\left(T_C^{FE} - T_C^{FM}\right)\right]^2}. \tag{26}$$

For temperatures $T_C^{FM} < T_C^{FE}$, the correction is twice smaller. The change of magnetization at the FE Curie point is

$$\Delta(M^2) = -\frac{\gamma_{||}\chi_{||} + \gamma_\perp\chi_\perp}{2\beta_M^*}. \tag{27}$$

We notice that even at the point of the FE-paraelectric phase transition the susceptibility $\hat{\chi}$ is finite supporting the assumption of weak spatial dispersion.

For large values of parameters γ and $R_{||,\perp}$, additional phase transitions may occur in the vicinity of the FE phase transition, see Fig. 5. The curves in Fig. 5 show the ME effect discussed in Refs. [32,33] using the microscopic theory. These curves are plotted for the same parameters as in Fig. 4(a), except $\gamma_{||} = -41$ and $\gamma_\perp = -2$.

The dielectric susceptibility $\hat{\chi}$ depends on the electric field E_0. Therefore the magnetic properties of the GFM film also depend on the electric field. Figure 6 shows the GFM magnetization vs the electric field E_0 at zero applied magnetic field. Figures 6(a) and 6(b) correspond to the different strengths of magnetoelectric coupling. Both figures are plotted for 47% Ni GFM placed above the colemanite FE substrate. The upper panel shows the case of weak interaction with parameters $\gamma_{||} = -24$ and $\gamma_\perp = -1.6$ and temperature $T = 80$ K. At this temperature the GFM film is in the ferromagnetic state. Applying electric field we change the dielectric permittivity of the FE substrate leading to a strong dependence of magnetization on the electric field. The dependence shows

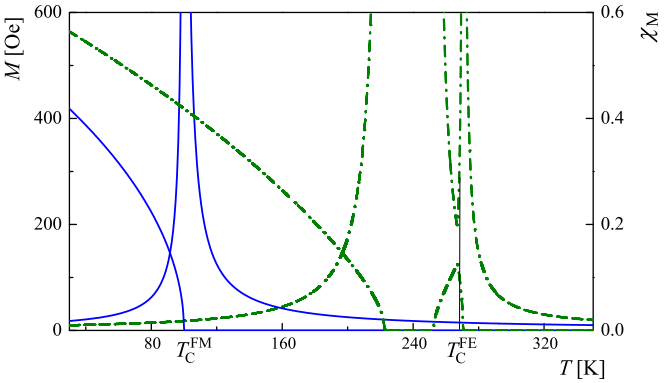

FIG. 5. (Color online) Magnetization M (solid blue line) and magnetic susceptibility χ_M (dashed red line) vs temperature at zero magnetic and electric fields and strong coupling between charge fluctuations and magnetization. Here, $T_C^{FE} < T_C^{FM}$, this limit corresponds to colemanite FE substrate and 45% of Ni granular film. Two additional phase transitions occur in the vicinity of the FE phase transition.

a hysteresis behavior similar to the dielectric permittivity field dependence.

Figure 6(b) shows the case of strong interaction, here, the parameters $\gamma_{||} = -41$, $\gamma_\perp = -1$, and temperature $T = 150$ K. In this case, the magnetic phase transition is induced when a strong electric field $E_0 = \pm E_m$ is applied.

B. Influence of GFM film on the FE layer

In this section, we investigate the influence of the magnetic subsystem on the FE layer. The correction to the polarization P quadratic in the electric induction $\mathbf{D}$ has the form

$$\mathbf{P}^{(2)} = -4\beta_P[(\hat{\chi}\mathbf{D})^2\hat{\chi}\mathbf{P}_0 + 2(\mathbf{P}_0\hat{\chi}\mathbf{D})\hat{\chi}\hat{\chi}\mathbf{D}]. \quad (28)$$

The correction $\mathbf{P}^{(2)}$ averaged over the FE volume is parallel to the polarization $\mathbf{P}_0$:

$$\langle\mathbf{P}^{(2)}\rangle = 4Q^2\beta_P\mathbf{P}_0\chi_\perp[3(\chi_\perp)^2R_\perp^* + (\chi_{||})^2R_{||}^*], \quad (29)$$

where $R_{\perp,||}^* = \Omega_{GFM}R_{\perp,||}/\Omega_{FE}$. Using Eq. (16) for the parameter Q, we find

$$\langle\mathbf{P}^{(2)}\rangle = \frac{4}{h}\left(Q_0^2 - \frac{\gamma M^2}{\alpha_Q}\right)\beta_P\mathbf{P}_0\chi_\perp(3\chi_\perp^2R_\perp^* + \chi_{||}^2R_{||}^*). \quad (30)$$

For temperatures $T > T_C^{FM}$, the correction $\mathbf{P}^{(2)}$ in the presence of an external magnetic field behaves as $\mathbf{P}^{(2)} \sim \chi_M^2B_{ext}^2$, while for temperatures $T < T_C^{FM}$, it has a hysteresis dependence on the magnetic field, B_{ext}. As it is shown in Sec. V, the correction to the polarization due to the influence of the magnetic subsytem can be of the order of 10^{-3}–10^{-2}.

C. Dependence of magnetoelectric coupling on the system parameters

We use the Ewald approach to calculate the electric field of a two-dimensional periodic lattice of quadrupoles [53]. The field produced by this lattice is periodic in the (x, y) plane and decays along the z direction. The spatial Fourier harmonics of

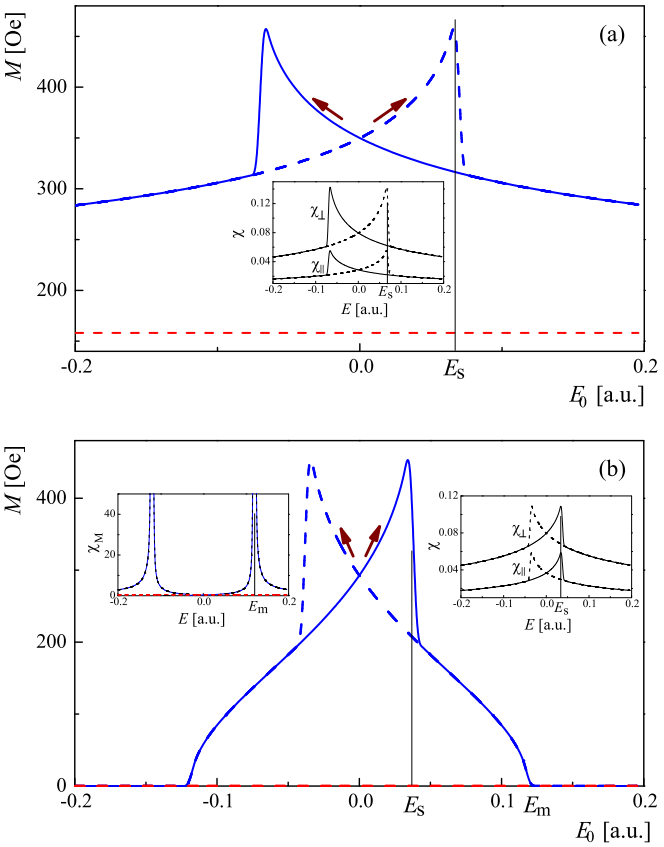

FIG. 6. (Color online) (a) Magnetization M vs electric field E_0 at zero magnetic field for colemanite FE and 47% of Ni GFM ($T_C^{FE} > T_C^{FM}$). Solid (blue) and dashed (blue) lines show the magnetization at finite interaction between the FE layer and the GFM film. Dotted (red) line describes the noninteracting case. (a) corresponds to the case of weak magnetoelectric coupling with the parameters $\gamma_{||,\perp}$ being -24 and -1.6, respectively. Temperature $T = 80$ K. Inset: dependence of $\chi_\perp$ and $\chi_{||}$ on the electric field E_0. E_s is the FE polarization switching field. (b) The case of strong coupling with $\gamma_{||} = -41$, $\gamma_\perp = -1$, and $T = 150$ K. Right inset: dependence of $\chi_\perp$ and $\chi_{||}$ on the electric field E_0. E_s is the FE polarization switching field, E_m is the electric field at which the magnetic phase transition occurs in the system. Left inset: magnetic susceptibility vs electric field.

the field are given by

$$E_{x,y}(\mathbf{k}_\perp, z) = i\sqrt{\frac{4\pi}{5}}\frac{\pi}{L_g^2}(k_{x,y})k_\perp E^{-k_\perp z} \times\left[\frac{2\cos(2\phi_\perp)}{\sqrt{6}}\left(Q_2^{(2)} + \tilde{Q}_2^{(2)}e^{i\mathbf{k}_\perp\mathbf{s}}\right) + Q_0^{(2)} + \tilde{Q}_0^{(2)}e^{i\mathbf{k}_\perp\mathbf{s}}\right],$$

$$E_z(\mathbf{k}_\perp, z) = -\sqrt{\frac{4\pi}{5}}\frac{\pi}{L_g^2}k_\perp^2E^{-k_\perp z} \times\left[\frac{2\cos(2\phi_\perp)}{\sqrt{6}}\left(Q_2^{(2)} + \tilde{Q}_2^{(2)}e^{i\mathbf{k}_\perp\mathbf{s}}\right) + Q_0^{(2)} + \tilde{Q}_0^{(2)}e^{i\mathbf{k}_\perp\mathbf{s}}\right], \quad (31)$$

where $\mathbf{k}_\perp = (k_x,k_y,0)$, $\phi_\perp = \arctan(k_x/k_y)$. The wave vector $\mathbf{k}_\perp$ has the discrete values $\mathbf{k}_\perp^{n,m} = (2\pi n/L_g, 2\pi m/L_g, 0)$. There are two quadrupoles, $\hat{Q}^1$ and $\hat{Q}^2$, in a unit cell. The vector $\mathbf{s}$ defines the shift of these dipoles, $\mathbf{s} = (\pi/L_g, \pi/L_g, 0)$. The parameters $Q_i^{(2)}$ and $\tilde{Q}_i^{(2)}$ are related to Q as follows: $Q_0^{(2)} = -Q$, $\tilde{Q}_0^{(2)} = -Q$, $Q_2^{(2)} = -3Q/(2\sqrt{6})$, $\tilde{Q}_2^{(2)} = 3Q/(2\sqrt{6})$.

The magnitude of the spatial Fourier harmonic in Eq. (31) decreases exponentially with increasing vector $k_\perp$. Therefore, even for $z = L_g$, we can neglect all harmonics except the four harmonics nearest to zero, $(\pm 2\pi/L_g, 0, 0)$ and $(0, \pm 2\pi/L_g, 0)$. Using Eq. (31), we obtain

$$
\begin{aligned}
&E_x(\pm 2\pi/L_g,0,z) \\
&\quad = \pm i\sqrt{\frac{4\pi}{5}}\frac{4\pi^3}{L_g^4}e^{-2\pi z/L_g} \\
&\qquad \times\left[\frac{2}{\sqrt{6}}\left(Q_2^{(2)} + \tilde{Q}_2^{(2)}e^{i\mathbf{k}_\perp\mathbf{s}}\right) + Q_0^{(2)} + \tilde{Q}_0^{(2)}e^{i\mathbf{k}_\perp\mathbf{s}}\right], \\
&E_y(\pm 2\pi/L_g,0,z) = 0, \\
&E_z(\pm 2\pi/L_g,0,z) \\
&\quad = -\sqrt{\frac{4\pi}{5}}\frac{4\pi^3}{L_g^4}e^{-2\pi z/L_g} \\
&\qquad \times\left[\frac{2}{\sqrt{6}}\left(Q_2^{(2)} + \tilde{Q}_2^{(2)}e^{i\mathbf{k}_\perp\mathbf{s}}\right) + Q_0^{(2)} + \tilde{Q}_0^{(2)}e^{i\mathbf{k}_\perp\mathbf{s}}\right], \\
&E_x(0, \pm 2\pi/L_g,z) = 0, \\
&E_y(0, \pm 2\pi/L_g,z) \\
&\quad = \pm i\sqrt{\frac{4\pi}{5}}\frac{4\pi^3}{L_g^4}e^{-2\pi z/L_g} \\
&\qquad \times\left[-\frac{2}{\sqrt{6}}\left(Q_2^{(2)} + \tilde{Q}_2^{(2)}e^{i\mathbf{k}_\perp\mathbf{s}}\right) + Q_0^{(2)} + \tilde{Q}_0^{(2)}e^{i\mathbf{k}_\perp\mathbf{s}}\right], \\
&E_z(0, \pm 2\pi/L_g,z) \\
&\quad = -\sqrt{\frac{4\pi}{5}}\frac{4\pi^3}{L_g^4}e^{-2\pi z/L_g} \\
&\qquad \times\left[-\frac{2}{\sqrt{6}}\left(Q_2^{(2)} + \tilde{Q}_2^{(2)}e^{i\mathbf{k}_\perp\mathbf{s}}\right) + Q_0^{(2)} + \tilde{Q}_0^{(2)}e^{i\mathbf{k}_\perp\mathbf{s}}\right]. \qquad (32)
\end{aligned}
$$

The amplitude of electric field oscillations decays with distance as $e^{-2\pi z/L_g}$. The parameter R is averaged over the volume of the FE ($d < z < h + d$). Using Eq. (32), we find

$$R_{||,\perp} \sim e^{-4\pi d/L_g}(1 - e^{-4\pi h/L_g}). \qquad (33)$$

The magnetoelectric coupling exponentially decays with increasing the distance between the GFM film and the FE layer with the characteristic decay length being the intergrain distance, L_g.

The coefficients R saturate with increasing FE thickness h due to the exponential decay of the electric field with distance d. The saturation occurs for thickness h larger than the intergrain distance L_g leading to the weak influence of the GFM film on the FE layer.

IV. FE WITH STRONG SPATIAL DISPERSION

A. Influence of FE layer on the GFM film

The coupling between the FE layer and the GFM film depends on the parameter R, see Eq. (14). Above, we discussed the case of a FE without spatial dispersion meaning that the FE response $\hat{\chi}(\mathbf{r},\mathbf{r}')$ is local. In the opposite case, of strong spatial dispersion, we can consider $\hat{\chi}(\mathbf{r},\mathbf{r}') = \text{const}$ being independent of coordinates. In this case, Eq. (14) has the form

$$R = R_0 - \left(\sum_i \int \mathbf{D}_i^q(\mathbf{r})d^3r\right)\frac{\hat{\chi}}{2\Omega_{GFM}}\left(\sum_j \int \mathbf{D}_j^q(\mathbf{r})d^3r\right). \qquad (34)$$

The average field created by the ensemble of quadrupoles is zero. Therefore, for strong spatial dispersion, the FE layer and the GFM film are decoupled since the parameter $R \to R_0$. Thus below we consider the quantity R with large but finite spatial dispersion.

The linear response of the FE layer is described by the following equation:

$$-\delta_P \Delta \mathbf{P}^{(1)} + \hat{\chi}^{-1}\mathbf{P}^{(1)} = \mathbf{D}. \qquad (35)$$

This equation differs from Eq. (20) by the term with spatial derivatives responsible for the dispersion. We use the following boundary condition for the polarization: $(P^{(1)})_z' = 0|_{z=h,h+d}$, with h and $h + d$ being the boundary positions of the FE layer [43,54,55].

It was shown in Sec. III C that the electric field $\mathbf{D}$ produced by the lattice of quadrupoles is periodic in the (x,y) plane and decays in the z direction. For distances $|z| > L_g$ away from the GFM film, the field has (x,y) spatial Fourier harmonics with only $|\mathbf{k}_\perp| = 2\pi/L_g$ and the decay length $k_d = 2\pi/L_g$. Such a field can be considered as a wave with zero wave vector $|\mathbf{k}|^2 = |\mathbf{k}_\perp|^2 - k_d^2 = 0$. Therefore the partial solution of Eq. (35) has the form

$$\mathbf{P}_p^{(1)} = \hat{\chi}\mathbf{D}, \qquad (36)$$

and the uniform solution has the form

$$\mathbf{P}_u^{(1)} = \mathbf{C}_1 e^{-\hat{\kappa}z} + \mathbf{C}_2 e^{\hat{\kappa}z}, \qquad (37)$$

where the vectors $\mathbf{C}_1$ and $\mathbf{C}_2$ depend on the x and y coordinates similar to the electric field $\mathbf{D}$:

$$\hat{\kappa} = \sqrt{\mathbf{k}_\perp^2 + \hat{\chi}^{-1}/\delta_P}; \qquad (38)$$

$\hat{\kappa}$ is a tensor. The appropriate components of tensor $\hat{\chi}^{-1}$ should be used for each vector component $\mathbf{C}_{1,2}$. Using the boundary conditions, we find the coefficients $\mathbf{C}_{1,2}$:

$$
\begin{aligned}
\mathbf{C}_1 &= \frac{k_\perp \hat{\chi}\tilde{\mathbf{D}}}{\hat{\kappa}(e^{\hat{\kappa}h} - e^{-\hat{\kappa}h})}e^{-k_\perp d - \hat{\kappa}d}(e^{-k_\perp h} - e^{-\hat{\kappa}h}), \\
\mathbf{C}_2 &= \frac{k_\perp \hat{\chi}\tilde{\mathbf{D}}}{\hat{\kappa}(e^{\hat{\kappa}h} - e^{-\hat{\kappa}h})}e^{-k_\perp d + \hat{\kappa}d}(e^{-k_\perp h} - e^{\hat{\kappa}h}). \qquad (39)
\end{aligned}
$$

Here, $\tilde{\mathbf{D}}$ is the part of the vector $\mathbf{D}$ that depends on the coordinates x and y only, $\tilde{\mathbf{D}} = e^{k_\perp z}\mathbf{D}$. For strong spatial dispersion and thick FE layer, the linear polarization has the

form

$$\mathbf{P}^{(1)} = \mathbf{P}_{\rm p}^{(1)} + \mathbf{P}_{\rm u}^{(1)} = \frac{\mathbf{D}}{2\delta_{\rm P} k_\perp^2} \times\left[(z-d)k_\perp + 1 - \frac{3 + 3(z-d)k_\perp + (z-d)^2 k_\perp^2}{4\chi\delta_{\rm P} k_\perp^2}\right]. \tag{40}$$

The characteristic length scale for the coefficients $R_{||,\perp}$ is the distance between two centers of neighboring grains $L_{\rm g}$ since the electric induction $\mathbf{D}$ in the FE layer decays exponentially. For estimates, we use $z - d \approx L_{\rm g}$ and $(z-d)k_\perp \approx 1$. Thus we find for the polarization

$$\mathbf{P}^{(1)} \approx \frac{\mathbf{D}}{\delta_{\rm P} k_\perp^2}\left(1 - \frac{7}{8\hat{\chi}\delta_{\rm P} k_\perp^2}\right). \tag{41}$$

Using Eq. (41), we calculate the coefficient R:

$$\begin{aligned} R &= \tilde{R}_0 - \frac{\tilde{R}_{||}}{\chi_{||}} - \frac{\tilde{R}_\perp}{\chi_\perp}, \\ \tilde{R}_0 &= R_0\left(1 + \frac{L_{\rm g}^2}{\delta_{\rm P} 4\pi^2}\right), \\ \tilde{R}_{||} &= -\frac{7L_{\rm g}^4 R_{||}}{8\delta_{\rm P}^2(4\pi^2)^2}, \\ \tilde{R}_\perp &= -\frac{7L_{\rm g}^4 R_\perp}{8\delta_{\rm P}^2(4\pi^2)^2}. \end{aligned} \tag{42}$$

The coefficient $R_{||,\perp}$ is calculated using Eq. (19) with electric field given by Eq. (32). It follows that the influence of the FE layer on the GFM film is suppressed for strong spatial dispersion by the factor $1/[\delta_{\rm P}(2\pi/L_{\rm g})^2]$. The coefficient $\tilde{R}_{||,\perp}$ have the opposite sign to the coefficient $R_{||,\perp}$.

The equation for the magnetization has the form

$$2\left(\tilde{\alpha}_{\rm M}^* + \frac{\tilde{\gamma}_\perp}{\chi_\perp} + \frac{\tilde{\gamma}_{||}}{\chi_{||}}\right)\mathbf{M} + 4\tilde{\beta}_{\rm M} M^2 \mathbf{M} = \mathbf{B}, \tag{43}$$

with the following coefficients:

$$\begin{aligned} \tilde{\alpha}_{\rm M}^* &= \alpha_{\rm M} - \gamma\tilde{R}_0 Q_0/\alpha_{\rm Q}, \\ \tilde{\gamma}_\perp &= \gamma\tilde{R}_\perp Q_0/\alpha_{\rm Q}, \\ \tilde{\gamma}_{||} &= \gamma\tilde{R}_{||} Q_0/\alpha_{\rm Q}. \end{aligned} \tag{44}$$

In contrast to the weak dispersion case, here the susceptibility χ is present in the denominator leading to a different dependence of the magnetization on the temperature and electric field.

Figure 7 shows the magnetization M behavior in the vicinity of the critical temperature $T_{\rm c}^{\rm FE}$ for strong spatial dispersion. All parameters for the GFM film are the same as before and we used the colemanite FE. According to Eq. (42), the magnetoelectric coupling coefficient $\tilde{\gamma}$ is the same as in the case of weak dispersion, however, it is multiplied by the small (in the case of strong spatial dispersion) parameter $(L^2/\delta_{\rm P} * 4\pi^2)$. Figure 7 demonstrates two different cases with $\delta_{\rm P} = 2$ and 10 nm^2. The first value of $\delta_{\rm P}$ corresponds to the case when the domain wall thickness in the FE $l_{\rm DW} \sim \sqrt{\chi\delta_{\rm P}}$ is slightly larger than the intergrain distance $L_{\rm g}$. The second

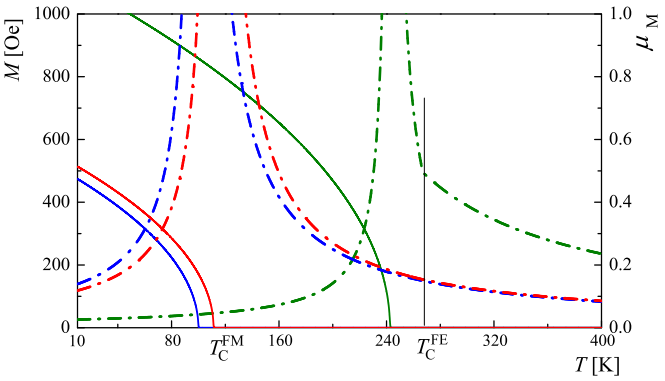

FIG. 7. (Color online) Magnetization M (solid lines) and magnetic susceptibility $\chi_{\rm M}$ (dash-dotted lines) vs temperature T for strong spatial dispersion and zero external magnetic and electric fields. Blue lines show the noninteracting case while the red and green lines correspond to the finite interaction of the FE layer with the GFM film. Red line is for $\delta_{\rm P} = 10$ nm^2. Green line is for $\delta_{\rm P} = 2$ nm^2.

case corresponds to $l_{\rm DW} \gg L_{\rm g}$, where the intergrain distance is $L_{\rm g} = 7$ nm.

In general, increasing the difference $|T - T_{\rm c}^{\rm FE}|$ one can study the crossover from strong to weak dispersion. Thus the dependence of the magnetization on the temperature can be considered as a combination of Figs. 4 and 7. The crossover temperature between two regimes depends on the system parameters.

The magnetization M versus electric field E_0 is shown in Fig. 8 for $T_{\rm c}^{\rm FM} < T_{\rm c}^{\rm FE}$ and fixed temperature $T = 245$ K. For FE substrate, we used the colemanite. The behavior is shown for small constant $\delta_{\rm P} = 2$ nm^2. In this limit, the domain wall thickness $l_{\rm DW} \sim \sqrt{\chi\delta_{\rm P}}$ is not too big in comparison with the intergrain distance, $L_{\rm g}$. Similar to the case of weak dispersion the FE substrate essentially influences the GFM magnetic state. Applying the electric field $E_{\rm m}$, one can induce the magnetic phase transition.

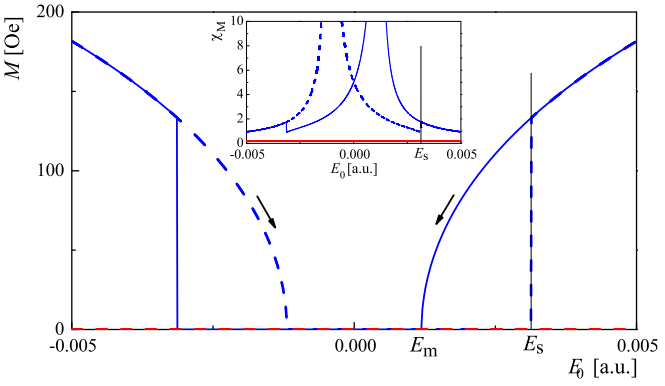

FIG. 8. (Color online) Magnetization M vs electric field E_0 for strong spatial dispersion and zero external magnetic field. Blue lines show two branches of magnetization for the case of finite interaction of the FE (colemanite) layer with the GFM film. Dashed red line corresponds to the noninteracting case. The plots are shown for the following sets of parameters: $T = 245$ K, $\delta_{\rm P} = 2$ nm^2. (Inset) Magnetic susceptibility $\chi_{\rm M}$ vs electric field E_0.

For thin FE layer, the polarization is given by

$$\mathbf{P}^{(1)} = \mathbf{P}_{\mathrm{p}}^{(1)} + \mathbf{P}_{\mathrm{u}}^{(1)} = \frac{\mathbf{D}}{\delta_{\mathrm{P}} k_{\perp}^2}\left(1 - \frac{1}{\hat{\chi}\,\delta_{\mathrm{P}} k_{\perp}^2}\right). \tag{45}$$

This polarization produces similar behavior of magnetization as a function of temperature and electric field with slightly modified coefficients. For thin FE film, the coefficients $\tilde{R}_{\perp,||}$ are linearly depend on the FE thickness h.

B. Influence of GFM film on the FE layer

In this section we investigate the influence of the GFM film on the FE layer in the case of strong dispersion. The equation describing the part of polarization quadratic in the electric induction has the form

$$-\delta_{\mathrm{P}}\Delta\mathbf{P}^{(2)} + (\hat{\chi})^{-1}\mathbf{P}^{(2)} = -4\beta_{\mathrm{P}}\,[2(\mathbf{P}_0\mathbf{P}^{(1)})\mathbf{P}^{(1)} + (\mathbf{P}^{(1)})^2\mathbf{P}_0]. \tag{46}$$

To solve Eq. (46), we use the same boundary conditions as we used before for $\mathbf{P}^{(1)}$. We are interested in the average polarization $\mathbf{P}^{(2)}$ appearing due to a nonlinear response. Only the average z component of $\mathbf{P}^{(2)}$ is nonzero. $P_z^{(2)}$ has a contribution with $\mathbf{k}_\perp = 0$. For this component, we have

$$\delta_{\mathrm{P}}\frac{\partial^2}{\partial z^2}P_z^{(2)} - (\hat{\chi})^{-1}P_z^{(2)} = \frac{4\beta_{\mathrm{P}}P_0}{(\delta_{\mathrm{P}}k_\perp^2)^2}\left(3\left\langle D_z^2\right\rangle_{x,y} + \left\langle \mathbf{D}_\perp^2\right\rangle_{x,y}\right). \tag{47}$$

Here, the notation $\langle\rangle_{x,y}$ stands for averaging over the (x,y) plane. The field $\mathbf{D}^2$ decays with distance as $e^{-2k_\perp z}$, where $k_\perp = 2\pi/L_{\mathrm{g}}$. Therefore the partial solution of Eq. (47) has the form

$$P_{z(\mathrm{p})}^{(2)} = \frac{\beta_{\mathrm{P}}P_0}{(\delta_{\mathrm{P}}k_\perp^2)^3}\left(3\left\langle D_z^2\right\rangle_{x,y} + \left\langle \mathbf{D}_\perp^2\right\rangle_{x,y}\right). \tag{48}$$

We neglect the term with the susceptibility $(\hat{\chi})^{-1}$ in Eq. (47). The uniform solution for $k_\perp = 0$ has the form

$$P_{z(\mathrm{u})}^{(2)} = C_1^z e^{\kappa^* z} + C_2^z e^{-\kappa^* z}, \tag{49}$$

where $\kappa^* = \sqrt{1/(\chi_{||}\delta_{\mathrm{P}})}$.

Using the boundary condition we find that $C_i^z \sim 1/(\delta_{\mathrm{P}}k_\perp^2)^{5/2}$ with $k_\perp = 2\pi/L_{\mathrm{g}}$. Therefore the average polarization $P_z^{(2)}$ decays with increasing the spatial dispersion as $(\delta_{\mathrm{P}}k_\perp^2)^{-5/2}$. For strong dispersion, the correction $P_z^{(2)}$ is also quadratic in parameter Q leading to the same behavior of average polarization on the magnetic field as in the case of weak dispersion. However, the influence of the GFM film on the FE layer is suppressed due to the spatial dispersion.

V. MICROSCOPIC MODEL OF MAGNETOELECTRIC COUPLING IN A COMBINED GFM SYSTEM

A. Direct effect: Influence of FE substrate on the GFM film

In Ref. [32], we developed the model describing the coupling between electric and magnetic degrees of freedom in the GMF. The coupling mechanism is based on the interplay of intergrain exchange coupling, Coulomb blockade, and screening of electric field by the FE polarization. In this model, the exchange interaction of two neighboring grains appears due to the overlap of electron wave functions in the space between the grains, see Fig. 3(b),

$$J \propto \sum \int \Psi_1^*(\mathbf{r}_2)\Psi_2^*(\mathbf{r}_1)U_c(\mathbf{r}_1 - \mathbf{r}_2)\Psi_1(\mathbf{r}_1)\Psi_2(\mathbf{r}_2)d\mathbf{r}_1 d\mathbf{r}_2. \tag{50}$$

Here, $\Psi_{1,2}$ is the spatial part of the electron wave function located in the first (second) grain; U_c is the Coulomb interaction of electrons located in different grains. The summation is over the different electron pairs in the grains:

$$\Psi_{1,2}(\mathbf{r}) = A\begin{cases} e^{-\frac{a}{\lambda}}, & |\mathbf{r} \pm \mathbf{L}_{\mathrm{g}}/2| < a, \\ e^{-\frac{|\mathbf{r}\pm\mathbf{L}_{\mathrm{g}}/2|}{\lambda}}, & |\mathbf{r} \pm \mathbf{L}_{\mathrm{g}}/2| > a. \end{cases} \tag{51}$$

Here, A is the normalization constant and L_{g} is the distance between two grain centers. λ is the electron localization length. It depends on the dielectric permittivity of the FE leading to the strong influence of the FE state on the intergrain exchange interaction and consequently on the magnetic state of the granular film [32].

In the simplest case, with small localization length, $\lambda < \min(a, L_{\mathrm{g}})$, the exchange interaction has the form $J \sim \lambda^2 e^{-\kappa L_{\mathrm{g}}/\lambda}$, where κ is a positive number of order one. At equilibrium, without FE, this expression can be linearized in ξ around ξ_0, $J = J_0 + (\lambda - \lambda_0)\tilde{\gamma}$, where ξ_0 is the localization length in the absence of a FE layer. Changing the localization length ξ, one can control the exchange interaction and thus the magnetic state of the granular film.

For small localization length, $\lambda \ll a$, one can calculate the quadrupole moment of two electrons between the grains, $Q_{xx} \sim \lambda a e$, $Q_{yy} = Q_{zz} = -1/2Q_{xx}$, $Q = Q_{xx} + Q_{yy} = 1/2Q_{xx}$. Calculating Q_{xx} we assumed that positively charged ions are located inside the grains and we averaged over the region between the centers of two grains, $-L_{\mathrm{g}}/2 < z < L_{\mathrm{g}}/2$, see Fig. 3(b). Thus the quadrupole moment Q is a linear function of localization length ξ and therefore the exchange interaction can be written as $J = J_0 + (Q - Q_0)\gamma$.

B. Estimate of parameter γ

The coupling between the electrical and the magnetic subsystems appears due to the influence of the FE response on the intergrain exchange constant J and therefore on the ordering temperature of the magnetic subsystem $T_{\mathrm{C}}^{\mathrm{FM}} = z_{\mathrm{c}}J/3$, where z_{c} is the coordination number. We use $z_{\mathrm{c}} = 4$. To estimate the constant γ, we use the microscopic theory of Ref. [33], in particular Eq. (5) of Ref. [33]. We assume the following parameters: the grain radius is 3 nm, the intergrain distance (the distance between grains centres) is 7 nm, the distance between the grain centers and the FE substrate surface is 4 nm. We assume that $\epsilon^{\mathrm{FE}} \gg \epsilon_{\mathrm{eff}}$, where ϵ_{eff} is the effective dielectric permittivity of the medium outside the FE substrate. The effective dielectric constant can be estimated as $\epsilon_{\mathrm{eff}} = 5$. For large ϵ^{FE}, one can expand Eq. (5) of Ref. [33] in the small parameter $\epsilon_{\mathrm{eff}}/\chi_0^{\mathrm{FE}}$. Using the above parameters, we find for the exchange constant $J \approx J_0(1 + \epsilon_{\mathrm{eff}}/\epsilon^{\mathrm{FE}})$. Matching this expression with Eq. (23) one can find $\gamma \approx \tilde{\alpha}^{\mathrm{FM}} T_{\mathrm{C}}^{\mathrm{FM}} 16\pi^2\epsilon_{\mathrm{eff}}$. This estimate is done for a rather small distance between the FE substrate and the magnetic film. Increasing the distance exponentially reduces the coupling constant γ.

C. Inverse effect: influence of GFM film on the FE substrate

In this section, we discuss the influence of the GFM film on the FE substrate and estimate the phenomenological constants α_Q and R. We assume that the formation of inhomogeneous charge distribution is related to the fact that the conduction electrons penetrate beyond the grain boundaries. Three factors influence the penetration depth: (1) the kinetic energy of electrons inside a grain $E_{\rm kin}$, (2) the potential energy of electrons outside the grain $U_{\rm pot}$, (3) and electron Coulomb interaction. The penetration of electrons outside a grain decreases the kinetic energy, but increases the potential $U_{\rm pot}$ and the Coulomb $E_{\rm Coul}$ energies. First, we neglect the influence of intergrain exchange interaction, the last term in Eq. (15).

The kinetic energy has the form

$$E_{\rm kin} = \frac{\hbar^2 (6\pi^2 N)^{5/3}}{20 m_e (a')^2}, \tag{52}$$

where N is the number of electrons in the grain, m_e is the electron mass, $a' = a + \lambda_e$ is the effective grain radius. The effective grain radius accounts for the fact that electrons penetrate outside the grain by the distance λ_e, which is the electron localization length.

The potential energy has the form

$$E_{\rm pot} = \frac{U(6\pi^2 N)^{5/3}\lambda_e^3}{10\pi^2 (a')^3}, \tag{53}$$

where U is the height of the potential barrier produced by the insulator between the grains. It accounts for a small penetration length λ_e and a small penetration probability which is proportional to λ^2.

The Coulomb interaction contributes to the total energy since the charge distribution is nonuniform:

$$E_{\rm Coul} = \frac{9 e^2 \lambda_e^2 N^2}{5 (a')^3}. \tag{54}$$

This expression has a transparent meaning: each electron produces a charge $e\lambda_e/a$ outside the grain. A charge of the same magnitude but of the opposite sign appears inside the grain. The characteristic size of the system is a.

Minimizing the total energy, $W_{Qt} = E_{\rm kin} + E_{\rm pot} + E_{\rm Coul}$, we estimate the equilibrium penetration depth (λ_0) and "stiffness" of quadrupole system, $2(\alpha_Q + R)$:

$$\lambda_0 = \frac{\frac{18}{5}(eN)^2 + \sqrt{\left(\frac{18 e^2 N^2}{5}\right)^2 + \frac{3\hbar^2 6\pi^2 N^{10/3} U}{25\pi^2 m_e}}}{(3/5\pi^2) U (6\pi^2 N)^{5/3}}. \tag{55}$$

For a potential barrier larger than the Coulomb interaction, this expression can be simplified leading to $\lambda_0 \to \sqrt{\pi^2\hbar^2/(3 m_e U)}$. For estimate, we use $E_F = 5$ eV with $k_F = 12$ nm^{-1}, particle diameter $2a = 5$ nm. For such a grain, the number of electrons is $N = 4\times 10^3$. We use $U = 6$ eV for the potential energy of an insulator. For the above parameters, the equilibrium penetration length is $\lambda_0 = 0.05$ nm. We note that the Coulomb and potential energies are of the same order for such particles. For bigger particles, the contribution of the Coulomb energy will be stronger leading to a stronger suppression of the penetration length. Thus the nonuniformity of electric charges increases with decreasing grain size.

We estimate the equilibrium quadrupole moment Q_0 for cubic grains with size $2a$ with a positively charged center ($-a < x,y,z < a$) and a negatively charge region around the grain. This region has a size λ_0. We calculate the quadrupole moment over the cubic region between two centers of neighboring grains. For small λ_0, we find

$$Q_0 = -2ea\lambda_0 \left[\frac{(L-a)^2}{2a^2} + \frac{L^3 - (L-a)^3}{12a^3} - \frac{11}{18} \right]. \tag{56}$$

The estimate gives $Q_0 = 2\times 10^{-38}$ C m^2. Such a quadrupole produces a rather strong electric field inside the FE substrate. Using Eq. (31) for 6-nm distance between the granular film and the FE substrate, we find $|E| \approx 3\times 10^4$ V/m.

The stiffness constant is defined by the second derivative of the total energy, $\partial^2 W_{Qt}/\partial\lambda^2 \approx 10^5$ J/m^2. The stiffness constant is rather large in the current model. If the exchange interaction is about 100 K, it can not essentially influence the quadrupole system. A relative correction to λ due to the magnetic subsystem can be of the order of 10^{-3}–10^{-2}. Thus the relative change of polarization from disordered to ordered state by applying an external magnetic field is less than 10^{-3}–10^{-2}.

It is important to mention here that the above estimate of λ_0 is the lowest estimate since we did not take into account the fact that λ depends on the electron energy. In particular, $\lambda > 0.1$ nm at the Fermi level. Electron transport measurements show that the penetration length at the Fermi level is about 0.5–1 nm meaning that electrons near the Fermi surface are responsible for the exchange coupling between the grains.

To summarize, the "direct" and "inverse" effects are strongly asymmetric. The direct effect can be rather strong, while the inverse effect is very weak. This is a consequence of the fact that the exchange interaction is weaker than the direct Coulomb interaction between quadrupoles in the GFM film with a FE layer.

VI. DISCUSSION

In this section, we discuss the validity of our model. The real granular films can not be described by the regular lattice since materials have always some degree of disorder. The quadrupole moments fluctuate in space, magnitude, and orientation due to this randomness. However, the presence of disorder does not change qualitatively our main results. In particular, the electric field produced by the GFM film decays exponentially with distance leading to the same results. The coupling between the GFM film and the FE layer decreases with increasing spatial dispersion of the FE layer. This effect is suppressed for FEs with domain wall thickness exceeding the average intergrain distance. For strongly disordered films, one can use a continuous spatial distribution of quadrupole moments. For a multilayer system of grains, only the nearest layer to the FE substrate will interact with the FE due to the exponential decay of coupling with distance.

In our consideration, we used a certain type of boundary conditions for FE polarization, with polarization derivatives being zero at the interface. In general, one can use the following combination for boundary conditions, $\zeta_1 P + \zeta_2 (P)'_z = 0$. It does not change qualitatively our results.

In this work, we discussed the case of an intrinsically isotropic dielectric which is typical for some organic components (such as TTF-CA). The only source of anisotropy in our consideration was the external electric field applied to the FE layer producing different susceptibilities—parallel $\chi_{||}$ and perpendicular $\chi_{\perp}$ to the layer surface. However, our considerations can be generalized for an intrinsically anisotropic FE. In this case, the final equations for the magnetization [see, for example, Eq. (23)] will be modified in the following way: instead of susceptibilities $\chi_{||}$ and $\chi_{\perp}$ defined in Eq. (22) one has to introduce the dielectric susceptibilities $\tilde{\chi}_{||}$ and $\tilde{\chi}_{\perp}$ which account for intrinsic anisotropy.

VII. CONCLUSION

We described the coupling between the FE polarization and the magnetization of a GFM film using a phenomenological model of a combined multiferroic system consisting of a granular ferromagnet film placed above the FE layer. We showed that the coupling is due to the presence of oscillating in space electric charges in the GFM film. On one hand, these charges interact with the FE layer via Coulomb interaction. On the other hand, they are coupled with the magnetization leading to the mutual influence of the FE polarization and the GFM film magnetization even for space a separated FE layer and GFM film. This model allows to study the importance of the spatial dispersion of the FE polarization and to understand the influence of the GFM film on the FE polarization.

We studied the temperature and electric field dependence of the magnetization and magnetic susceptibility of GFM film for weak and strong spatial dispersion of the FE layer. We calculated the electric polarization as a function of temperature and magnetic field and investigated the influence of the FE state on the magnetization and magnetic susceptibility and vice versa. The effect of mutual influence decreases with increasing spatial dispersion of the FE layer. For weak dispersion, the strongest coupling occurs in the vicinity of the FE-PE phase transition. For strong dispersion the situation is the opposite. We showed that for temperatures $T < T_C^{FE}$ the magnetization has a hysteresis as a function of the electric field. For strong coupling, the interaction of the FE layer and the GFM film leads to the appearance of an additional magnetic phase transition. Below the ordering temperature of GFM film, the FE polarization has hysteresis as a function of the magnetic field.

We studied the behavior of the magnetoelectric coupling as a function of the distance between the FE layer and the GFM film. We showed that for large distances the coupling decays exponentially due to the exponential decrease of the electric field produced by the oscillating charges in the GFM film.

We showed that the magnetoelectric coupling depends on the thickness of the FE layer. For thin layers, it grows linearly and saturates for thickness exceeding some critical value.

ACKNOWLEDGMENT

I.B. was supported by NSF under Cooperative Agreement Award EEC-1160504, NSF Award DMR-1158666, and NSF PREM Award.

[1] W. Eerenstein, N. D. Mathur, and J. F. Scott, Nature (London) **442**, 759 (2006).
[2] R. Ramesh and N. A. Spaldin, Nat. Mater. **6**, 21 (2007).
[3] M. Bibes and A. Barthelemy, Nat. Mater. **7**, 425 (2008).
[4] R. Ramesh, Nature (London) **461**, 1218 (2009).
[5] J. T. Heron, J. L. Bosse, Q. He, Y. Gao, M. Trassin, L. Ye, J. D. Clarkson, C. Wang, J. Liu, S. Salahuddin, D. C. Ralph, D. G. Schlom, J. Inigues, B. D. Huey, and R. Ramesh, Nature (London) **516**, 370 (2014).
[6] S.-W. Cheong and M. Mostovoy, Nat. Mater. **6**, 13 (2007).
[7] S. M. Wu, S. A. Cybart, D. Yi, J. M. Parker, R. Ramesh, and R. C. Dynes, Phys. Rev. Lett. **110**, 067202 (2013).
[8] V. Laukhin, V. Skumryev, X. Marti, D. Hrabovsky, F. Sanchez, M. V. Garcia-Cuenca, C. Ferrater, M. Varela, U. Luders, J. F. Bobo, and J. Fontcuberta, Phys. Rev. Lett. **97**, 227201 (2006).
[9] H. Ohno, D. Chiba, F. Matsukura, T. Omiya, E. Abe, T. Dietl, Y. Ohno, and K. Ohtani, Nature (London) **408**, 944 (2000).
[10] D. Chiba, M. Sawicki, Y. Nishitani, Y. Nakatani, F. Matsukura, and H. Ohno, Nature (London) **455**, 515 (2008).
[11] D. Chiba, M. Yamanouchi, F. Matsukura, and H. Ohno, Science **301**, 943 (2003).
[12] H. Katsura, N. Nagaosa, and A. V. Balatsky, Phys. Rev. Lett. **95**, 057205 (2005).
[13] I. A. Sergienko and E. Dagotto, Phys. Rev. B **73**, 094434 (2006).
[14] C.-W. Nan, Phys. Rev. B **50**, 6082 (1994).
[15] C. Thiele, K. Dorr, O. Bilani, J. Rodel, and L. Schultz, Phys. Rev. B **75**, 054408 (2007).
[16] S. Geprags, A. Brandlmaier, M. Opel, R. Gross, and S. T. B. Goennenwein, Appl. Phys. Lett. **96**, 142509 (2010).
[17] M. Weisheit, S. Fahler, A. Marty, Y. Souche, C. Poinsignon, and D. Givord, Science **315**, 349 (2007).
[18] M. Tsujikawa and T. Oda, Phys. Rev. Lett. **102**, 247203 (2009).
[19] C.-G. Duan, J. P. Velev, R. F. Sabirianov, Z. Zhu, J. Chu, S. S. Jaswal, and E. Y. Tsymbal, Phys. Rev. Lett. **101**, 137201 (2008).
[20] M. Y. Zhuravlev, S. Maekawa, and E. Y. Tsymbal, Phys. Rev. B **81**, 104419 (2010).
[21] V. Garcia, M. Bibes, L. Bocher, S. Valencia, F. Kronast, A. Crassous, X. Moya, S. Enouz-Vedrenne, A. Gloter, D. Imhoff, C. Deranlot, N. D. Mathur, S. Fusil, K. Bouzehouane, and A. Barthelemy, Science **327**, 1106 (2010).
[22] C. Jia and J. Berakdar, Phys. Rev. B **80**, 014432 (2009).
[23] C. Jia and J. Berakdar, Phys. Rev. B **83**, 045309 (2011).
[24] G. A. Smolenskii and I. E. Chupis, Sov. Phys. Usp. **25**, 475 (1982).
[25] Y. J. Choi, H. T. Yi, S. Lee, Q. Huang, V. Kiryukhin, and S.-W. Cheong, Phys. Rev. Lett. **100**, 047601 (2008).
[26] J. H. Park, H. H. Shin, and H. M. Jang, Phys. Rev. B **77**, 212409 (2008).
[27] M. Liu, X. Li, J. Lou, S. Zheng, K. Du, and N. X. Sun, J. Appl. Phys. **102**, 083911 (2007).
[28] H. Ryu, P. Murugavel, J. H. Lee, S. C. Chae, T. W. Noh, Y. S. Oh, H. J. Kim, K. H. Kim, J. H. Jang, M. Kim, C. Bae, and J.-G. Park, Appl. Phys. Lett. **89**, 102907 (2006).

[29] J. G. Wan, X. W. Wang, Y. J. Wu, M. Zeng, Y. Wang, H. Jiang, W. Q. Zhou, G. H. Wang, and J.-M. Liu, Appl. Phys. Lett. **86**, 122501 (2005).
[30] T. D. Thanh, P. T. Phong, D. H. Manh, N. V. Khien, L. V. Hong, T. L. Phan, and S. C. Yu, J. Mater. Sci.: Mater. Electron **24**, 1389 (2013).
[31] X. L. Zhong, J. B. Wang, M. Liao, G. J. Huang, S. H. Xie, Y. C. Zhou, Y. Qiao, and J. P. He, Appl. Phys. Lett. **90**, 152903 (2007).
[32] O. G. Udalov, N. M. Chtchelkatchev, and I. S. Beloborodov, Phys. Rev. B **89**, 174203 (2014).
[33] O. G. Udalov, N. M. Chtchelkatchev, and I. S. Beloborodov, Phys. Rev. B **90**, 054201 (2014).
[34] M. Huth, A. Rippert, R. Sachser, and L. Keller, Mater. Res. Expr. **1**, 046303 (2014).
[35] O. G. Udalov, N. M. Chtchelkatchev, and I. S. Beloborodov, J. Phys.: Condens. Matter **27**, 186001 (2014).
[36] K. V. Reich, T. Chen, and B. I. Shklovskii, Phys. Rev. B **89**, 235303 (2014).
[37] S. A. Fedorov, A. E. Korolkov, N. M. Chtchelkatchev, O. G. Udalov, and I. S. Beloborodov, Phys. Rev. B **89**, 155410 (2014).
[38] S. A. Fedorov, A. E. Korolkov, N. M. Chtchelkatchev, O. G. Udalov, and I. S. Beloborodov, Phys. Rev. B **90**, 195111 (2014).
[39] L. G. Gerchikov, C. Guet, and A. N. Ipatov, Phys. Rev. A **66**, 053202 (2002).
[40] L. D. Landau and E. Lifshitz, *Course of Theoretical Physics: Electrodynamics of Continuous Medie* (Pergamon Press, 1960), Vol. 8.
[41] A. F. Devonshire, Phil. Magaz. **40**, 1040 (1949).
[42] B. A. Strukov and A. P. Levanyuk, *Ferroelectric Phenomena in Crystals* (Springer, Heidelberg, 1998).
[43] L.-H. Ong, J. Osman, and D. R. Tilley, Phys. Rev. B **63**, 144109 (2001).
[44] P. Chandra and P. B. Littlewood, in *Physics of Ferroelectrics* (Springer, Berlin, 2007), pp. 69–116.
[45] J. I. Gittleman, Y. Goldstein, and S. Bozowski, Phys. Rev. B **5**, 3609 (1972).
[46] S. Barzilai, Y. Goldstein, I. Balberg, and J. S. Helman, Phys. Rev. B **23**, 1809 (1981).
[47] K. Kimura and H. Ohigashi, Appl. Phys. Lett. **43**, 834 (1983).
[48] T. Yamada and T. Kitayama, J. Appl. Phys. **52**, 6859 (1981).
[49] J. B. Torrance, J. E. Vazquez, J. J. Mayerle, and V. Y. Lee, Phys. Rev. Lett. **46**, 253 (1981).
[50] E. Fatuzzo, J. Appl. Phys. **31**, 1029 (1960).
[51] H. H. Wieder, J. Appl. Phys. **30**, 1010 (1959).
[52] K. Kobayashi, S. Horiuchi, R. Kumai, F. Kagawa, Y. Murakami, and Y. Tokura, Phys. Rev. Lett. **108**, 237601 (2012).
[53] T. H. M. V. D. Berg and A. V. D. Avoird, Chem. Phys. Lett. **160**, 223 (1989).
[54] V. M. Fridkin, Sov. Phys. Usp. **49**, 193 (2006).
[55] V. M. Fridkin, R. V. Gaynutdinov, and S. Ducharme, Sov. Phys. Usp. **53**, 199 (2010).